

# *Vertical structure of stratospheric water vapour trends derived from merged satellite data*

Article

Accepted Version

Hegglin, M.I., Plummer, D.A., Shepherd, T.G., Scinocca, J.F., Anderson, J., Froidevaux, L., Funke, B., Hurst, D., Rozanov, A., Urban, J., von Clarmann, T., Walker, K.A., Wang, H.J., Tegtmeier, S. and Weigel, K. (2014) Vertical structure of stratospheric water vapour trends derived from merged satellite data. *Nature Geoscience*, 7 (10). pp. 768-776. ISSN 1752-0894 doi: <https://doi.org/10.1038/ngeo2236> Available at <http://centaur.reading.ac.uk/37807/>

It is advisable to refer to the publisher's version if you intend to cite from the work.

To link to this article DOI: <http://dx.doi.org/10.1038/ngeo2236>

Publisher: Nature Publishing Group

All outputs in CentAUR are protected by Intellectual Property Rights law, including copyright law. Copyright and IPR is retained by the creators or other copyright holders. Terms and conditions for use of this material are defined in the [End User Agreement](#).

[www.reading.ac.uk/centaur](http://www.reading.ac.uk/centaur)

## **CentAUR**

Central Archive at the University of Reading

Reading's research outputs online

1 *Vertical structure of stratospheric water vapour trends derived from merged*  
2 *satellite data*

3  
4 M. I. Hegglin, D. A. Plummer, T. G. Shepherd, J. F. Scinocca, J. Anderson, L. Froidevaux,  
5 B. Funke, D. Hurst, A. Rozanov, J. Urban, T. von Clarmann, K. A. Walker, R. Wang, S.  
6 Tegtmeier, and K. Weigel

7  
8 **Stratospheric water vapour is a powerful greenhouse gas and knowledge of its**  
9 **long-term behaviour is crucial to understand climate change. The longest**  
10 **available record from balloon observations over Boulder shows increases in**  
11 **stratospheric water vapour which cannot be fully explained by observed**  
12 **changes in its main drivers, tropical tropopause temperatures and methane.**  
13 **Although satellite observations could help resolve the conundrum,**  
14 **constructing a reliable long-term data record is challenging. Here we**  
15 **introduce a new data merging approach using a chemistry-climate model**  
16 **nudged to observed meteorology as a transfer function between satellite**  
17 **datasets, overcoming issues arising from instrument drifts and short overlap**  
18 **periods. In the lower stratosphere, the resulting water-vapour record is**  
19 **extended back to 1988 and largely follows tropical tropopause temperatures.**  
20 **Lower and mid-stratospheric long-term trends are negative rather than**  
21 **positive, with Boulder trends shown not to be globally representative. In the**  
22 **upper stratosphere, the record is extended back to 1986 and shows positive**  
23 **long-term trends. The altitudinal differences in the trends are explained by**  
24 **methane oxidation together with a strengthened lower-stratospheric and**  
25 **weakened upper-stratospheric circulation inferred by this analysis. Our**  
26 **results call into question previous estimates of surface radiative forcing based**  
27 **on presumed long-term global lower-stratospheric water-vapour increases.**

28  
29 Recent experiences with climate data records suggest that there is nothing like ‘the  
30 ultimate climate data record’ and that different approaches to dataset construction  
31 are needed to estimate the uncertainty introduced by the construction process itself.  
32 For example, upper-tropospheric warming was underestimated by Microwave-  
33 Sounding Unit Channel 2 temperature due to the influence of a priori information  
34 and the coarse vertical resolution of the retrieval<sup>1</sup>. More recently, it has been  
35 argued<sup>2</sup> that the apparent hiatus in global-mean warming is an artefact of sampling  
36 biases in the global network of surface data used to estimate global mean  
37 temperature changes. Both examples illustrate the limitations of observational  
38 datasets with gaps filled by statistical relationships.

39  
40 An important climate data record is stratospheric water vapour, which exerts a  
41 strong radiative forcing affecting temperatures both locally<sup>3</sup> and at Earth’s  
42 surface<sup>4,5</sup>. Through thermal-wind balance, stratospheric temperature changes are  
43 believed to affect the stratospheric circulation and, through dynamical coupling,  
44 surface climate<sup>6,7</sup>. Long-term changes in extratropical lower-stratospheric water  
45 vapour derived from balloon measurements at Boulder (the longest available  
46 record<sup>8</sup>) from 1980-2010 show an average increase of  $1.0 \pm 0.2$  ppmv in the 16-26

47 km altitude range<sup>9,10</sup>. About 25-30% of this increase has been attributed to methane  
48 oxidation<sup>10,11</sup>. The rest remains unexplained, since tropical tropopause  
49 temperatures (another key driver of long-term changes<sup>12</sup>) exhibit trends that are  
50 not significantly different from zero over this period<sup>13,14</sup>. Comparison of the Boulder  
51 record with HALOE satellite measurements, which exhibit essentially a zero long-  
52 term trend from 1992-2005, shows discrepancies in the early 1990s<sup>15</sup>. However,  
53 there is a possibility that the HALOE record suffers from aerosol contamination or  
54 long-term drifts<sup>16</sup>.

55

56 The observed records of stratospheric water vapour thus present a conundrum. As a  
57 result, confidence in global long-term trends is low<sup>17,18</sup>. The difficulty in quantifying  
58 stratospheric water-vapour trends arises from limitations of observational systems  
59 in the face of strong interannual and decadal variability<sup>15,19,20</sup>. There is general  
60 agreement that upper-tropospheric and lower-stratospheric humidity  
61 measurements from the global radiosonde network cannot be trusted<sup>21</sup>. Balloon-  
62 borne frostpoint hygrometers are characterized by high accuracy and precision<sup>22</sup>,  
63 but their measurement records are temporally and spatially sparse. Satellite  
64 instruments offer global coverage but have finite lifetimes, so different datasets  
65 need to be merged into long-term records, often without much overlap. Even with  
66 overlapping datasets, the merging may introduce temporal inhomogeneities since  
67 aging instruments can show degradation in performance.

68

### 69 **New approach to merge stratospheric water vapour datasets**

70

71 We introduce a new approach to investigate long-term trends in stratospheric water  
72 vapour, using timeseries from a state-of-the art chemistry-climate model nudged to  
73 observed meteorology (but not water vapour) from the ERA-Interim reanalysis over  
74 1980-2010 (CMAM30) as a transfer function between satellite datasets. This  
75 approach exploits the extensive effort made in developing stable reanalysis  
76 products, with ERA-Interim now exhibiting a much better representation of the  
77 stratospheric circulation than earlier products<sup>21</sup>. The resulting CMAM30  
78 stratospheric water vapour is expected to provide a reasonable long-term reference  
79 since it includes the main known transport, mixing, microphysical (dehydration at  
80 the tropical tropopause and in polar regions), and chemical processes (in particular  
81 methane oxidation) affecting its distribution and long-term changes. Although the  
82 model is not assumed to be correct in absolute terms, its use as a transfer function  
83 allows relative biases between satellite instruments to be determined using all  
84 available measurements, not just those restricted to overlap periods, thereby  
85 improving the characterization of inter-instrument biases and allowing the  
86 identification of potential instrumental drifts or sampling issues. Consistency  
87 between model and measurements suggests that the processes controlling  
88 stratospheric water vapour are sufficiently well understood to explain the long-term  
89 changes, and that CMAM30 can be trusted as a transfer function, while  
90 inconsistencies point out weaknesses either in the model or observations. The  
91 temporal homogeneity of the water-vapour record can also be tested by examining  
92 the consistency of its long-term changes with those of other variables. Using this

93 knowledge, the observational datasets can more confidently be used to create long-  
94 term data records.

95  
96 As an application of the approach, we merge zonal monthly-mean water-vapour  
97 timeseries from seven limb-viewing satellite instruments compiled and quality  
98 assessed by the SPARC Data Initiative<sup>23</sup> into a long-term record. *Figure 1a* shows the  
99 individual satellite timeseries at 100 hPa for 20S-20N and the large discrepancies  
100 between them. Relative biases to CMAM30 are calculated for each instrument  
101 (*Figure 1b*), avoiding periods where the instruments have known problems (see  
102 Supplementary Material). The post-2006 period is excluded from the relative-bias  
103 calculation because of a known inhomogeneity in ERA-Interim lower-stratospheric  
104 temperatures in late 2006 due to the introduction of GPS radio-occultation data<sup>24</sup>  
105 (see *Supplementary Material, Table 1*). Overall, the relative biases are seen to be well  
106 defined (as shown in scatter plots in *Supplementary Figure S1*), yielding confidence  
107 in the ability of CMAM30 to represent water-vapour variability, and thus in its use as  
108 a transfer function between datasets. Using CMAM30 as a transfer function, each  
109 instrument record is then adjusted relative to Aura-MLS (*Figure 1d*).

110  
111 There is a potential pitfall in this approach in that long-term changes in the merged  
112 dataset could be influenced by the long-term trend in the model. This possibility is  
113 assessed by examining whether there are apparent drifts in the model-  
114 measurement differences over time, or jumps between the older (SAGE II and  
115 HALOE) and newer instruments following the bias correction (*Figure 1c*). For the  
116 most part, the differences between these bias-corrected timeseries and CMAM30 are  
117 stable in time, suggesting that there is no artificial long-term trend introduced by  
118 this procedure. That the differences are stable over the SAGE II record furthermore  
119 indicates very good long-term stability of these observations, despite earlier  
120 concerns about a drift in the instrument's retrieval channel<sup>25</sup>. This suggests that  
121 SAGE II can be used to extend the satellite water-vapour record back to the mid-  
122 1980s. Distinct low biases are found for HALOE during 1993-1995, which are likely  
123 due to aerosol interference in the retrieval after the Mt. Pinatubo eruption, and  
124 during 2003-2005, confirming previous comparisons<sup>16,20</sup>. Similarly, the last year of  
125 SAGE II data (2005) seems to exhibit a low bias. The earlier MIPAS data (2002-  
126 2004) indicate a slight low bias with respect to the later MIPAS data (2005-2010), as  
127 also found in Ref 23. The remaining fluctuations reveal mostly differences in how  
128 the instruments resolve the amplitude of the seasonal cycle, likely attributable to  
129 differing vertical resolutions of the observations<sup>23</sup>. The bias-corrected timeseries  
130 show a coherent evolution of tropical lower-stratospheric water vapour (*Figure 1d*),  
131 with no evidence of a jump between the older and newer instruments — further  
132 evidence that the procedure has not introduced any artificial long-term trend. A  
133 merged satellite stratospheric water-vapour record is finally produced by  
134 calculating the multi-instrument mean of all available bias-corrected datasets  
135 (however excluding HALOE during 2003-2005 and SAGE II during 2005 due to their  
136 identified low biases).

137  
138

139 **Consistency with tropical tropopause temperatures**

140

141 In the lower stratosphere, water vapour is known to broadly follow variations in  
142 tropical tropopause temperatures<sup>15,16,17,19,20,27,28</sup>. The merged record is therefore  
143 compared to temperature fluctuations, using deseasonalized anomalies normalized  
144 by the standard deviation of the respective variable's interannual variability in  
145 order to make them comparable and check their consistency (*Figure 2a*). We here  
146 use the CMAM30 100 hPa temperature averaged over 15S-15N, which has been  
147 shown to vary coherently with cold-point tropopause temperatures<sup>19,28</sup>, and  
148 emphasize again that the variability and trends of the individual datasets are  
149 unaffected by the bias correction and thus not influenced by the model. The 80 hPa  
150 water-vapour anomalies derived from the merged satellite record (at this level  
151 representative of purely stratospheric air) strongly follow the temperature  
152 fluctuations, with a correlation coefficient (R) (or variance explained) of 0.77 (59%)  
153 over the full time period, which increases to 0.89 (78%) when considering only  
154 2001 onwards (likely explained by the better spatio-temporal coverage provided by  
155 the newer instruments, resulting in more representative zonal monthly means). The  
156 consistency between the temperature and water-vapour datasets is further  
157 highlighted by plotting the normalized differences (or residuals) of their anomalies  
158 (*Figures 2b and c*), for which the inter-annual variability is much reduced.

159 Consistency between the merged water-vapour record and tropical tropopause  
160 temperatures is also found in the extratropical lower stratosphere at 100 hPa (with  
161 a lag of two months to account for transport time scales between the tropics and  
162 extratropics<sup>28</sup>)(*Figures 2d and e*), with a correlation coefficient (variance explained)  
163 of 0.66 (43%). The normalized differences between water vapour and temperature  
164 are somewhat stronger than in the tropics, due to enhanced dynamical variability  
165 and its effect on tracer transport and mixing with older stratospheric air at these  
166 latitudes. Dehydration in the polar vortex may also contribute<sup>29</sup>. The good  
167 agreement between measurements and model (*Figure 2e*) shows that these  
168 additional processes are adequately represented in the model. Nevertheless, the  
169 low-frequency variability of extratropical lower-stratospheric water vapour seems  
170 mainly to arise from the variability of tropical tropopause temperatures.

171

172 There are four time periods that show deviations from this strong correlation: 1992-  
173 1996 for the observations (but not for the model), which is presumed to be a result  
174 of Mt Pinatubo aerosol affecting the water-vapour retrieval<sup>16</sup>; and 1999-2000, 2003,  
175 and 2008-2009. The causes of the latter are not known but since they occurred in  
176 both observations and model they are presumed to be real.

177

178 The new merged water-vapour record appears to be an improvement over a  
179 previous merge of the HALOE and Aura-MLS data sets based only on the relative  
180 bias during their 16 months of overlap<sup>16,17,30</sup>, since the latter record shows a  
181 temporal inhomogeneity in deviations from the temperature record (*Figures 2c,e*).  
182 As discussed above, HALOE exhibits a low bias in the lower stratosphere during its  
183 final years of operation that may adversely affect a long-term data record

184 constructed by merging HALOE with another dataset such as Aura-MLS during this  
185 period. Our approach, in contrast, shows that taking the long-term behaviour of the  
186 datasets into account substantially improves the consistency between the water-  
187 vapour and temperature records. After the strong dip around 2001, the previous  
188 merge of HALOE and Aura-MLS only partially recovers by 2010 (Refs 30,31), while  
189 the merged record using CMAM30 recovers fully to pre-2001 values by 2007.  
190 Calculations of surface radiative forcing from changes in lower-stratospheric water  
191 vapour based on the simple merge of HALOE and Aura-MLS<sup>30</sup> may thus  
192 overestimate the cooling effect on global mean surface temperatures after 2001.

### 193 194 195 **Comparison with in-situ observations over Boulder**

196  
197 We now turn to the question of the apparent inconsistency between the long-term  
198 Boulder FPH balloon and satellite datasets<sup>15,17</sup>. We investigate whether the Boulder  
199 trends are representative of the Northern Hemisphere mid-latitude stratosphere by  
200 sub-sampling the model at the location (40N/105W) and time of the Boulder  
201 measurements. *Figure 3a* shows Boulder 100 hPa water-vapour anomalies  
202 extending back to 1980 together with the full and subsampled anomalies derived  
203 from the model. The agreement between the merged satellite and full model  
204 datasets back to 1988 provides confidence that the model exhibits a correct  
205 representation of inter-annual variability and long-term changes in stratospheric  
206 water vapour. The sub-sampled model fields generally correlate better with the  
207 Boulder in-situ measurements than do the full model fields in terms of year-to-year  
208 fluctuations, explaining the differences between the Boulder and (zonal-mean)  
209 satellite observations during some years (e.g., 1988-1992, 1997-1998, and 2003-  
210 2005). Nevertheless, the 100 hPa change over 1980-2010 derived from the sub-  
211 sampled model fields ( $-0.27 \pm 0.18$  ppmv) disagrees with that from Boulder ( $0.6 \pm 0.15$   
212 ppmv). The difference is smaller, but still statistically significant ( $-0.15 \pm 0.22$  ppmv  
213 compared with  $0.39 \pm 0.18$  ppmv), over 1988-2010 where the zonal-mean model  
214 trend is consistent with that of the merged satellite record. The differences from the  
215 near-global water-vapour fields (*Figure 3b*) illustrate in more detail the close  
216 agreement between the sub-sampled and Boulder water-vapour records, except for  
217 the three time periods highlighted in red which together lead to the differences in  
218 their long-term trends. Inspection of the model's longitude-latitude distribution of  
219 water-vapour changes indicates that these are not longitudinally uniform (*Figure*  
220 *3c*). Positive trends are found south-west of Boulder, with the limited spatial  
221 resolution of the model likely missing the full extent of the geographical structure  
222 and temporal variability of this feature. Our results suggest that the water-vapour  
223 trends over Boulder should not be considered representative of the global  
224 stratosphere.

### 225 226 **Long-term stratospheric water-vapour changes**

227

228 *Figure 4a* shows the bias-corrected individual water-vapour datasets at 10 hPa in  
229 the extratropics together with the model-instrument biases (*Figure 4b*). Our method  
230 reveals minor discrepancies between two available SAGE II data versions (see  
231 Supplementary Material). HALOE shows no apparent low bias as was identified in  
232 the lower stratosphere for its last years of operation, showing that satellite  
233 instrument biases and drifts can be latitude- and altitude-dependent. While the  
234 model exhibits a strong low bias at this altitude, its long-term evolution and inter-  
235 annual variability show very good agreement with the observations back to 1986  
236 (*Figure 4c*). This level of agreement provides confidence in the ERA-Interim  
237 reanalysis driving the model while at the same time highlighting once again the high  
238 quality of the SAGE II data, suggesting that the satellite water-vapour record can be  
239 extended back to the mid-1980s. (See *Supplementary Figure S3* for more examples.)  
240

241 *Figure 5a* shows the long-term changes between the late 1980s and 2010 derived  
242 from the merged satellite record throughout the stratosphere, and *Table 1* quantifies  
243 the long-term changes shown in the different figures. The trends are significantly  
244 positive in the upper stratosphere, while the lower and mid-stratosphere show  
245 significant negative trends (in contrast to the Boulder observations). This vertical  
246 structure in the long-term trends is found at all latitudes. In the tropical tropopause  
247 region around 80 hPa, a negative long-term trend is identified with 70%  
248 significance. On the other hand, positive changes of more than 10% are found in the  
249 tropical upper troposphere. While these latter two findings need to be treated with  
250 caution due to sampling limitations, they are in broad agreement with past trends  
251 derived from chemistry-climate model simulations<sup>12,32</sup>.  
252

253 The observed water-vapour changes are now attributed to different drivers using  
254 the well-established “total water” diagnostic<sup>33,34,16</sup> (see *Methods* and *Supplementary*  
255 *Material*). The contribution from methane entry-value changes is shown in *Figure*  
256 *5b*, and is derived from tropospheric observations of methane changes together with  
257 a fractional-release factor ( $\alpha$ ) (*Supplementary Figure S3*) inferred from ACE-FTS  
258 stratospheric methane measurements. The contribution varies smoothly from zero  
259 in the tropical lower stratosphere to approximately 3% of water vapour in the  
260 upper stratosphere, the latter representing a significant fraction of the observed  
261 water-vapour increase (*Figure 5a*). The contribution from water-vapour entry-value  
262 changes is obtained from the merged 80 hPa record shown in *Figure 2a*, and is a  
263 constant  $-0.14 \pm 0.2$  ppmv (hence not plotted). Assuming conservation of total water,  
264 the difference between the sum of those two contributions and the observed change  
265 can be attributed to changes in  $\alpha$ , representing a change in stratospheric circulation,  
266 whose inferred contribution to the observed water-vapour change is shown in  
267 *Figure 5c*. This contribution is negative in the lower stratosphere and positive in the  
268 upper stratosphere. The breakdown of the different contributions is shown in *Figure*  
269 *5d* together with their uncertainties for three locations with particularly large long-  
270 term water-vapour changes. The uncertainty in the inferred contribution from  
271 circulation changes is dominated by the large uncertainty in the water-vapour  
272 entry-value changes because of the large inter-annual variability of the latter (*Figure*



273 2a). However, the difference between the inferred contributions in the upper and  
274 lower stratosphere is robust because the same water-vapour entry-value change is  
275 used for both, and it is not possible to explain the observed water-vapour changes,  
276 within uncertainties, without the inferred circulation changes. In the northern high-  
277 latitude upper stratosphere (5 hPa, 62.5N) the long-term increase of 0.28 ppmv is  
278 due in equal measure to methane increase and  $\alpha$  increase, with an offset from the  
279 decreasing water-vapour entry value. In the midlatitude lower stratosphere of both  
280 hemispheres (30 hPa, 42.5N and 50 hPa, 43.5S), long term decreases of -0.28 and -  
281 0.34 ppmv respectively are mainly explained by decreasing  $\alpha$ , with an additional  
282 contribution from the decreasing water-vapour entry value and a small offset from  
283 the methane increase. Thus, the different drivers affect the water-vapour changes  
284 differently in different regions.

285  
286 Larger  $\alpha$  corresponds to older age-of-air. To facilitate comparison with observed  
287 estimates of long-term circulation changes, we determine an approximate  
288 relationship between the two quantities (*Supplementary Figure S5*), and use it to  
289 translate the inferred  $\alpha$  changes into age-of-air changes (*Figure 5e*). This shows a  
290 strong decrease in age-of-air in the lower stratosphere, and a weak increase in the  
291 upper stratosphere, which is broadly consistent with the evidence for both  
292 tendencies in long-term observations of stratospheric trace gases<sup>35,36,37</sup>. An  
293 increased strength of the lower-stratospheric circulation is also consistent with  
294 chemistry-climate model simulations<sup>38</sup>, likely exacerbated in past decades by the  
295 effect of the ozone hole, which will reverse sign in the future<sup>39</sup>.

### 296 297 **Improved knowledge of stratospheric water-vapour changes**

298  
299 We have introduced a novel method to generate a long-term record of stratospheric  
300 water vapour, using a chemistry-climate model nudged to observed meteorology to  
301 provide a transfer function between the available satellite datasets. This approach  
302 provides an improved assessment of the relative biases between instruments,  
303 potential instrumental drifts, as well as possible sampling biases, compared to what  
304 is possible from the observations alone, especially for instruments with no or small  
305 overlap in time.

306  
307 The new merged satellite water-vapour record extends back to the late 1980s and  
308 shows long-term decreases in the lower and mid-stratosphere, in contrast to the  
309 Boulder record which is shown not to be globally representative. Upper-  
310 stratospheric water vapour instead shows a long-term increase. The contributions  
311 of the two recognized drivers of water-vapour changes — the stratospheric entry  
312 values of water vapour and of methane — are quantified and shown not to be  
313 sufficient to explain the observed water-vapour trends, particularly the difference in  
314 the trends between the upper and lower stratosphere. The discrepancy is attributed  
315 to changes in the fractional-release factor between methane and water vapour,  
316 which imply a strengthened lower-stratospheric circulation (reduced age-of-air)  
317 and a weakened upper-stratospheric circulation (increased age-of-air), consistent

318 with other evidence. It hence appears necessary to consider long-term changes in  
319 the stratospheric circulation when interpreting changes in stratospheric water  
320 vapour, together with changes in methane and water-vapour entry values.

321  
322 Our results show the value of using models and measurements together to  
323 understand the interannual and long-term behaviour of stratospheric water vapour,  
324 with the approach being applicable in principle to other trace gases. They also  
325 highlight the need for independent and redundant global measurement systems  
326 characterized by high long-term accuracy (and precision) to be able to quantify  
327 long-term changes in stratospheric water vapour with more confidence.

328

329

### 330 **Acknowledgements**

331

332 We acknowledge the Canadian Space Agency for having funded the CMAM30  
333 project, with additional institutional support from the Canadian Centre for Climate  
334 Modelling and Analysis who provided the model code and supercomputing time. We  
335 thank all national and international space agencies for making available their limb  
336 satellite observations for use in the SPARC Data Initiative.

337

338

### 339 **Author contributions**

340

341 M.I.H. designed the methodology, performed the data analysis, and wrote the paper.  
342 D.A.P. helped with the statistical analysis and together with J.F.S. devised and  
343 implemented the nudged model simulations. T.G.S contributed to the interpretation  
344 and writing of the text. D. H. provided processed balloon observations. J. A., L. F., B.  
345 F., A. R., J. U., T. v. C., H. J. W., K. A. W., S. T. and K. W. processed and provided the  
346 satellite datasets.

347

### 348 **Additional information**

349

350 Supplementary material is provided. Correspondence and request for materials  
351 should be addressed to M.I.H.

352

### 353 **Competing financial interests**

354

355 The authors declare no competing financial interests.

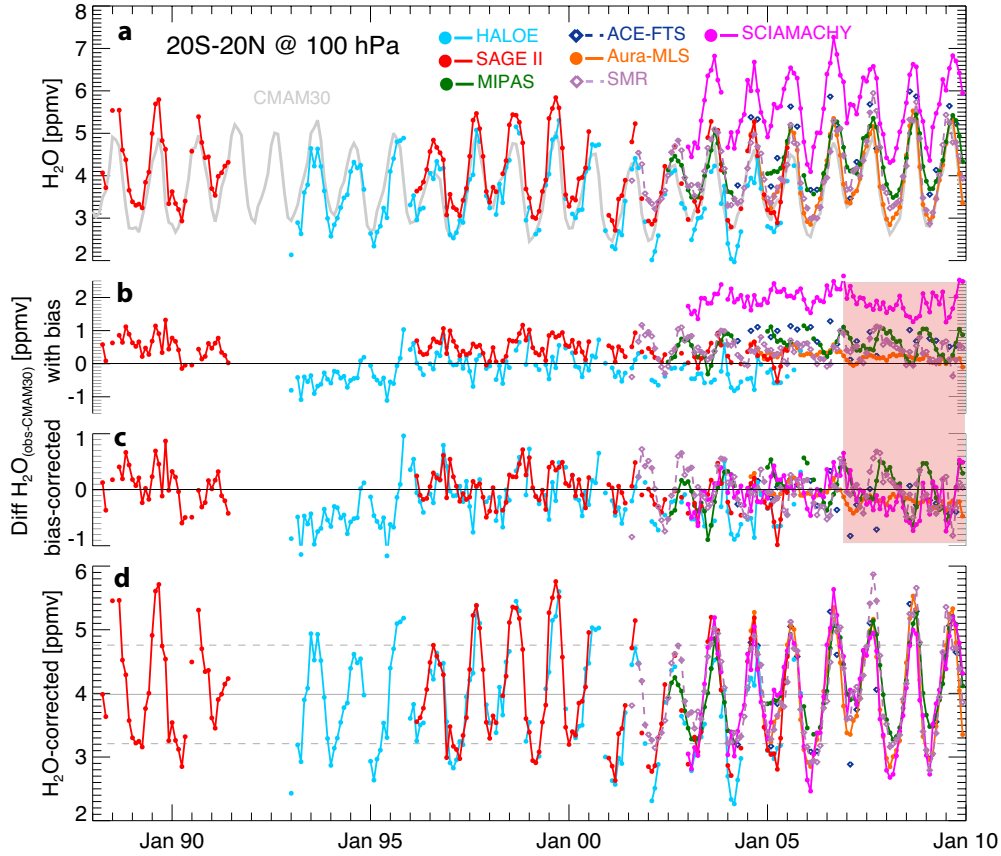
356

357

358

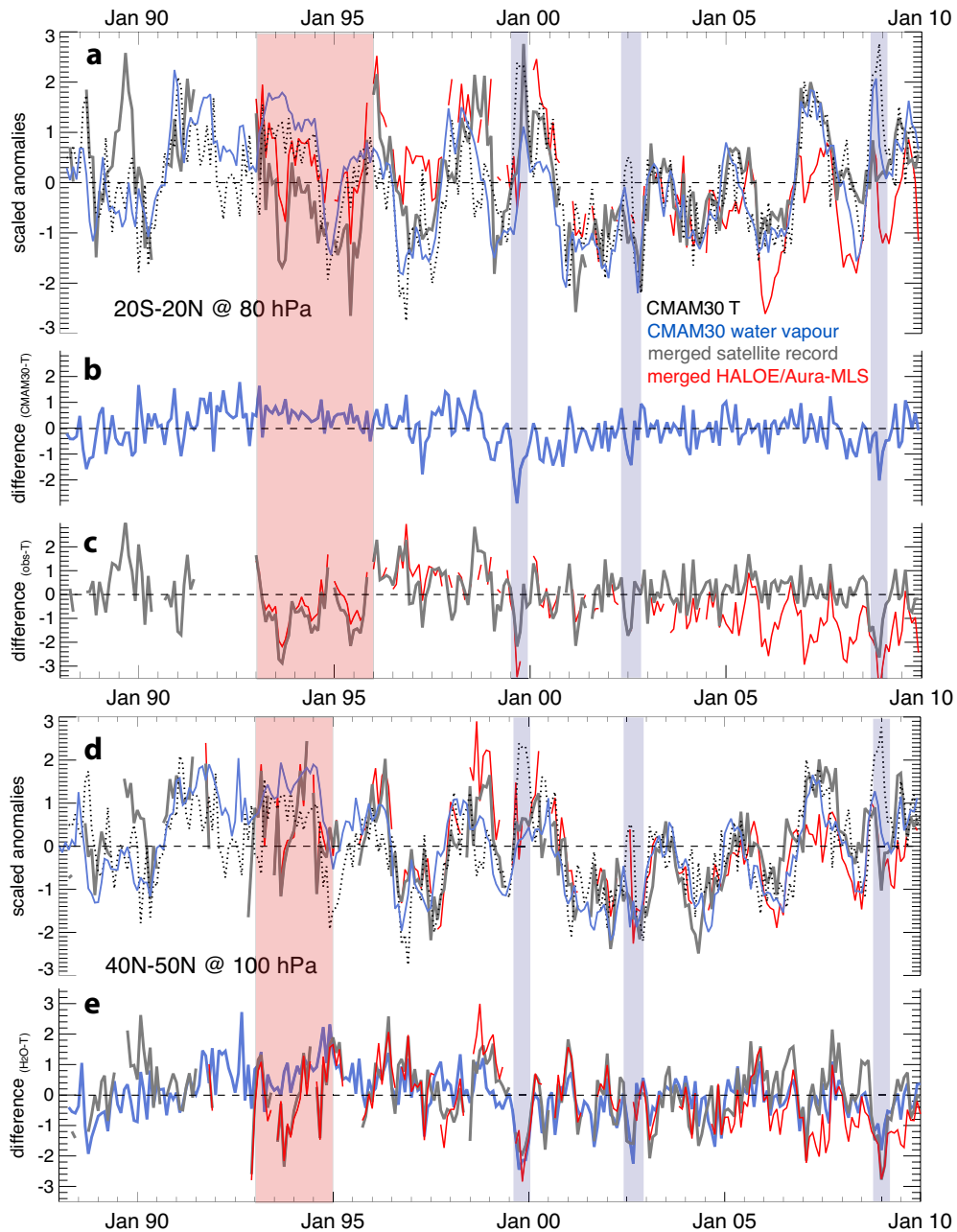
358  
359  
360  
361  
362

## FIGURES



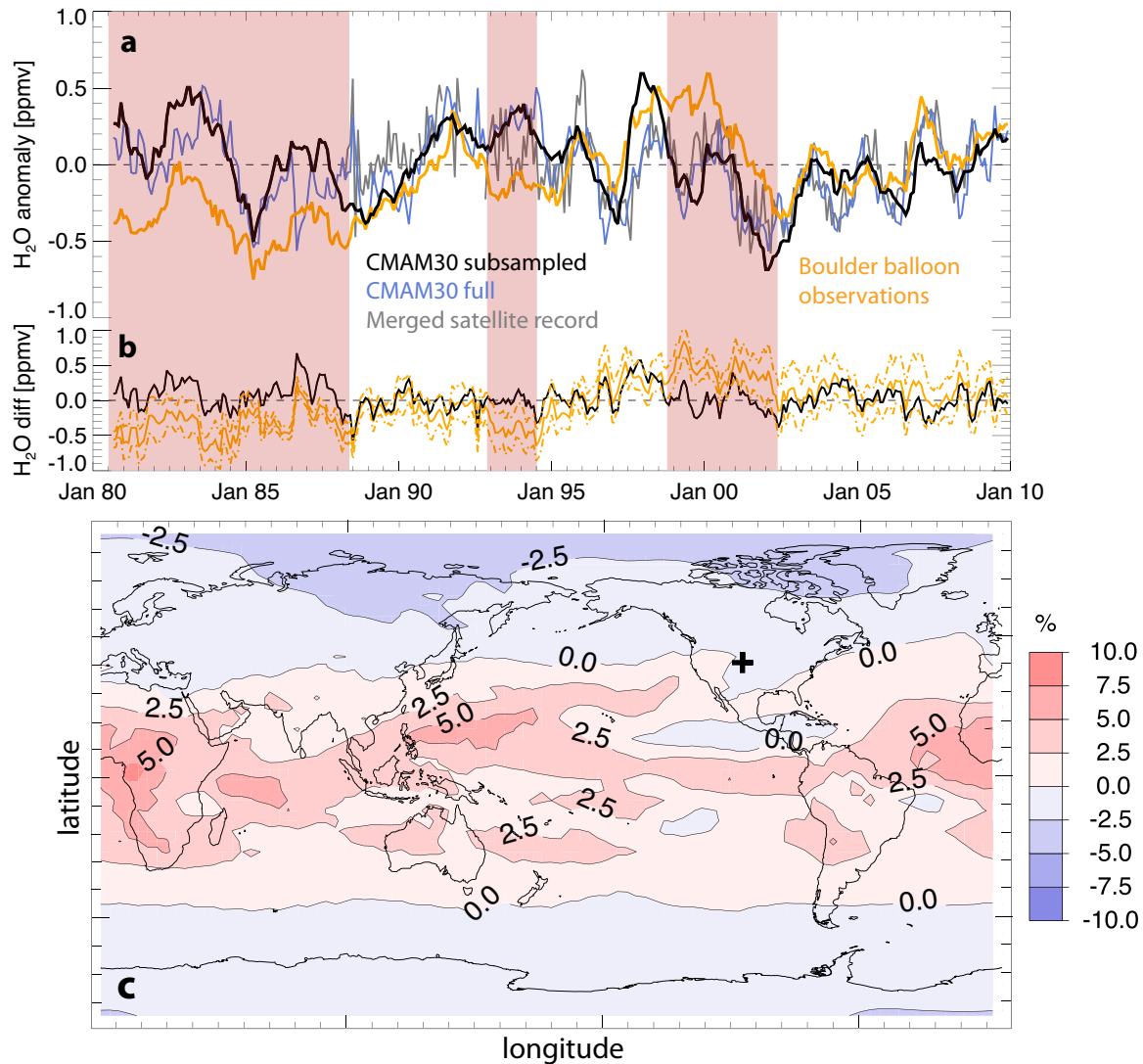
363  
364  
365  
366  
367  
368  
369  
370  
371  
372  
373  
374  
375

**Figure 1: Approach to merging a climate data record.** Timeseries of monthly zonal mean water vapour at 100 hPa averaged over 20S-20N for 1988-2010: **(a)** Absolute mixing ratios from different instruments (colours) and CMAM30 (grey), **(b)** differences and **(c)** bias-corrected differences between observations and CMAM30, and **(d)** bias-corrected absolute mixing ratios from observations. Grey solid and dashed horizontal lines in (d) indicate mean and 1-sigma standard deviation of the observational record averaged over the whole time period. The red box encompasses months excluded from the relative-bias determination due to identified problems in ERA-Interim (see text). See Supplementary Material for SCIAMACHY bias explanation.



376  
 377  
 378  
 379  
 380  
 381  
 382  
 383  
 384  
 385  
 386  
 387  
 388

**Figure 2: Consistency between tropical tropopause temperature and lower-stratospheric water vapour.** Scaled anomalies (unitless) of tropical temperature at 100 hPa averaged over 15S-15N and of water vapour at **(a)** 80 hPa averaged over 20S-20N and **(d)** 100 hPa averaged over 40N-50N. Tropical temperature is lagged by 2 (3) months in the tropics (extratropics). **(b, c, and d)** Differences between scaled temperature and water-vapour anomalies (unitless). Red bar highlights a time period where the scaled anomalies in the model and the observations show a substantial disagreement, blue bars where the temperature-water vapour relationship is strongly perturbed in both model and observations.



389

390

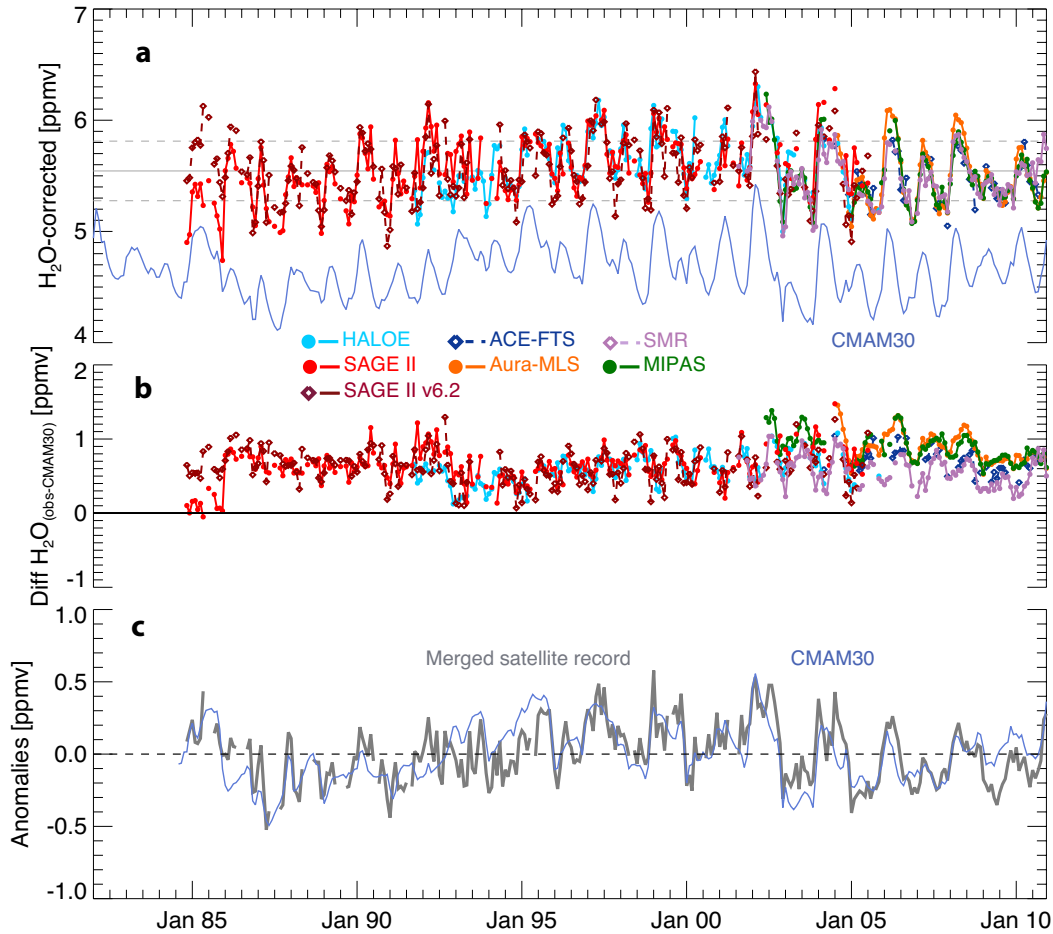
391 **Figure 3: Comparison of stratospheric water vapour from Boulder balloon and**392 **merged satellite datasets. (a) Deseasonalized water-vapour anomalies at 100 hPa**393 **derived from Boulder balloon observations (orange), the zonal mean (40N-50N)**394 **model (blue) and merged satellite data (grey), and the model subsampled at Boulder**395 **(black). (b) Differences between full model anomalies and balloon (orange) or sub-**396 **sampled model anomalies (black). Red shadings highlight periods where sub-**397 **sampled model data systematically lie outside the 1-sigma uncertainty of the**398 **balloon observations (dashed orange lines). (c) Longitude-latitude percentage**399 **changes of water vapour at 100 hPa for 1980-2010 from the model. The cross**400 **indicates the location of Boulder (40N/105W).**

401

402

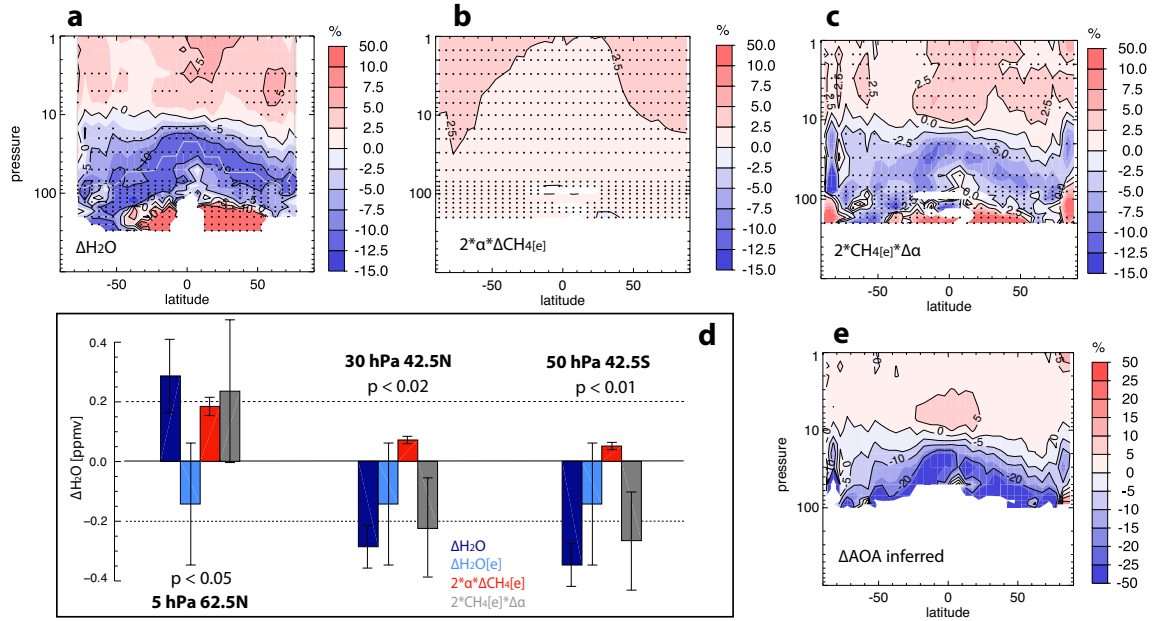
403

404



405  
 406  
 407  
 408  
 409  
 410  
 411  
 412  
 413

**Figure 4: Extension of the water-vapour timeseries back to the mid 1980s. (a)** Timeseries of zonal mean water vapour at 10 hPa and 40N for model (grey) and the different instruments (bias-corrected and colour-coded). **(b)** Relative biases between each instrument's original monthly zonal mean timeseries and CMAM30. **(c)** Deseasonalized anomalies of the merged satellite water-vapour record (grey) and the model.



414  
 415 **Figure 5: Long-term changes in stratospheric water vapour and its drivers. (a)**  
 416 Percentage changes up to 2010 derived from the merged satellite record since  
 417 1986/1988 above/below grey line. Dots indicate 95%-significance level.  
 418 Contribution to (a) from (b) tropospheric methane increases and (c) inferred  
 419 changes in the stratospheric circulation. (d) Absolute water-vapour changes at  
 420 three locations and contributions from their drivers including uncertainties (as  
 421 discussed in detail in *Supplementary Material*). P-values are given for the difference  
 422 between observed changes and the sum of the two entry-value contributions. (e)  
 423 Fractional-release factor changes translated into age-of-air (AOA) changes  
 424 (significance not estimated).

425  
 426  
 427 **Table 1: (a) Water vapour and (b) temperature changes derived for different**  
 428 **time periods, latitude bands, and altitudes from observations and from**  
 429 **CMAM30.** Changes are calculated for the timeseries shown in *Figures 2, S1, 3, and 5*  
 430 and given as total change in ppmv over the entire period. Most trends are not  
 431 statistically significant due to large variability in stratospheric water vapour when  
 432 compared to data record length. Decadal fluctuations strongly affect derived trend  
 433 values depending on the time period chosen<sup>10,31</sup>. Trend and significance calculation  
 434 is explained in the Methods section. *CMAM30ss* denotes sub-sampled model fields.  
 435

H <sub>2</sub> O	Period	Lat Band	Height [hPa]	Change [ppmv]	2-sigma Uncertainty [ppmv]	t-value	Effective Sample #	Significance Level
<b>Figures 2 and S1</b>								
Satellite	1988-2010	20S-20N	80	-0.14	0.20	0.67	26	70%
Satellite	1988-2010	20S-20N	100	0.01	0.14	0.06	53	Not sig

<b>Figure 3</b>								
Satellite	1988-2010	37.5-42.5N	100	-0.05	0.17	0.27	32	Not sig
Boulder	1988-2010	37.5-42.5N	100	0.39	0.18	2.17	129	95%
CMAM30ss	1988-2010	37.5-42.5N	100	-0.15	0.22	0.66	84	Not sig
CMAM30	1988-2010	37.5-42.5N	100	-0.07	0.22	0.32	16	Not sig
<b>Figure 4</b>								
Boulder	1980-2010	37.5-42.5N	100	0.60	0.15	3.9	160	95%
CMAM30ss	1980-2010	37.5-42.5N	100	-0.27	0.18	1.49	110	90%
CMAM30	1980-2010	37.5-42.5N	100	-0.12	0.19	0.64	22	Not sig
<b>Figure 5e</b>								
Satellite	1986-2010	62.5N	5	0.28	0.12	2.4	26	95%
Satellite	1986-2010	42.5N	30	-0.28	0.07	4.1	65	95%
Satellite	1986-2010	42.5S	50	-0.34	0.07	5.2	72	95%
Temp	Period	Lat Band	Height [hPa]	Change [K]	2-sigma Uncertainty [K]	t-value	Effective Sample #	Significance Level
<b>Figure 2</b>								
Model	1988-2010	15S-15N	100	-0.04	0.32	0.13	249	Not sig

436  
437  
438  
439



439 **Methods**

440

441 ***Nudged Chemistry-Climate Model simulations***. The CMAM30 dataset is produced  
442 using the Canadian Middle Atmosphere Model<sup>40</sup> driven by the latest European  
443 Centre for Medium-Range Weather Forecasts (ECMWF) ERA-Interim reanalysis<sup>21</sup>  
444 over the past 30 years (1980-2010). For details on the nudging see *Supplementary*  
445 *Material*. The model was run on 71 vertical levels from the surface to around 95 km,  
446 with a vertical resolution of approximately 1 km around the tropopause, and a  
447 horizontal resolution of T47, or approximately 4 degrees. The stratospheric source  
448 gas of water vapour, methane, is prescribed as a time-varying, global average  
449 surface concentration based on observations and is subject to model transport and  
450 chemistry. Water vapour is likewise a fully prognostic field in the model, chemically  
451 produced by methane oxidation and removed through parameterized large-scale  
452 and deep convective precipitation processes. Water vapour in excess of the local  
453 saturation mixing ratio is removed, following the rationale that the stratospheric  
454 water-vapour entry value is largely determined by the Lagrangian cold point as air  
455 passes through the tropical tropopause<sup>19</sup>, but neglecting super-saturation<sup>41</sup>. The  
456 free-running CMAM has been evaluated for its performance in the upper  
457 troposphere and lower stratosphere both in the tropics<sup>12</sup> and extratropics<sup>42</sup> and  
458 found to be one of the best-performing models. CMAM30 data can be downloaded  
459 from [http://www.cccma.ec.gc.ca/data/cmam/output/CMAM/CMAM30-](http://www.cccma.ec.gc.ca/data/cmam/output/CMAM/CMAM30-SD/index.shtml)  
460 [SD/index.shtml](http://www.cccma.ec.gc.ca/data/cmam/output/CMAM/CMAM30-SD/index.shtml)

461

462 ***SPARC Data Initiative timeseries***. The SPARC Data Initiative water-vapour  
463 timeseries have been compiled using profile data that were carefully screened  
464 before binning, and a hybrid log-linear interpolation in the vertical has been  
465 performed. The timeseries feature zonal monthly mean cross sections with a  
466 horizontal resolution of 5° on 28 pressure levels between 300 and 0.1 hPa (around  
467 64 km altitude). We here use the timeseries from seven instruments, which provide  
468 near-global coverage (SAGE II, HALOE, Odin/SMR, SCIAMACHY, ACE-FTS, Aura-MLS,  
469 and MIPAS) and have been quality-assessed within the SPARC Data Initiative<sup>23</sup>.  
470 Sampling issues are discussed in Ref 43. The climatologies were based on the  
471 following data versions (specific references are provided in Ref 23): HALOE v19,  
472 SMR v2.0 (in the lower stratosphere) and SMR v2.1 (in the middle and upper  
473 stratosphere), SCIAMACHY v3.0, ACE-FTS v2.2, Aura-MLS v3.3, and MIPAS  
474 v3o\_H2O\_13 (for 2002-2004 data) and v5r\_H2O\_220 (for 2005-2010 data, where  
475 the operation mode was switched from high-spectral to low-spectral resolution).  
476 SAGE II v6.2 submitted to the SPARC Data Initiative is only shown in *Figure 4*, but  
477 otherwise is superseded by climatologies based on the improved SAGE II v7.0  
478 data<sup>43</sup>. For methane, ACE-FTS data<sup>45</sup> were used. The SPARC Data Initiative  
479 climatologies can be downloaded from [http://www.sparc-climate.org/data-](http://www.sparc-climate.org/data-center/data-access/sparc-data-initiative/)  
480 [center/data-access/sparc-data-initiative/](http://www.sparc-climate.org/data-center/data-access/sparc-data-initiative/)

481

482 ***Boulder balloon observations***. Water vapour vertical profile measurements over  
483 Boulder by balloon-borne NOAA frost point hygrometers (FPHs) started in April  
484 1980 and continue today. Most soundings were conducted monthly, however the

485 record contains several multi-month data gaps, especially above 22 km. A  
486 comparison of FPH and Aura-MLS measurements over Boulder and Lauder, New  
487 Zealand, shows no significant temporal drifts between the two instruments from  
488 100 to 26 hPa during 2004-2012 (Ref. 46). See also discussion of measurement  
489 uncertainty in the *Supplementary Material*.

490

491 **Anomalies.** Anomalies are calculated with respect to the full time period depicted in  
492 the different figures, by subtracting the seasonal cycle derived from each individual  
493 instrument or the model from the overall time series.

494

495 **Trends and significance tests.** Unless indicated otherwise, uncertainty estimates  
496 are given as two sigma throughout the manuscript. We use a least-square linear  
497 regression in order to derive the trends from deseasonalized water-vapour anomaly  
498 timeseries at the different altitudes and latitudes. The significance of the trend is  
499 derived taking into account the effect of potential autocorrelation within the  
500 timeseries on the number of independent data points (reducing the effective sample  
501 size). This effective sample size is then used to recalculate the uncertainty of the  
502 derived trends and determine the tabulated one-sided student's t-test value, used to  
503 define the significance level of the trends. A more detailed discussion of the method  
504 can be found in Ref 47.

505

506 **Total-water diagnostic.** Apart from polar dehydration and other non-conservative  
507 processes, stratospheric "total water"  $\text{H}_2\text{O} + 2 \cdot \text{CH}_4$  is approximately conserved<sup>33,34,16</sup>  
508 hence water vapour and methane at a given location can be written as

509

$$510 \text{H}_2\text{O} = \text{H}_2\text{O}_{[e]} + 2\alpha\text{CH}_{4[e]}, \quad \text{CH}_4 = (1-\alpha) \text{CH}_{4[e]} \quad (1a,b)$$

511

512 where the subscript '[e]' refers to the entry value at the tropical tropopause (lagged  
513 by the mean age-of-air), and  $\alpha$  represents a fractional-release factor which depends  
514 on the circulation. Under this assumption, sufficiently small water-vapour changes  
515 can be attributed to changes in water-vapour entry value, methane entry value, and  
516 circulation according to

517

$$518 \Delta\text{H}_2\text{O} = \Delta\text{H}_2\text{O}_{[e]} + 2\alpha\Delta\text{CH}_{4[e]} + 2\text{CH}_{4[e]}\Delta\alpha. \quad (2)$$

519

520 The calculation of  $\alpha$  and  $\Delta\text{CH}_{4[e]}$  and their uncertainties is described in the  
521 *Supplementary Material*. The last term in (2) is calculated as a residual of the other  
522 terms that can be derived from observations with its uncertainty being  
523 overwhelmingly dominated by that of  $\Delta\text{H}_2\text{O}_{[e]}$ . Hence the other uncertainties  
524 (including possible non-conservation of total water) are not critical.

525

525  
526  
527  
528  
529  
530  
531  
532  
533  
534  
535  
536  
537  
538  
539  
540  
541  
542  
543  
544  
545  
546  
547  
548  
549  
550  
551  
552  
553  
554  
555  
556  
557  
558  
559  
560  
561  
562  
563  
564  
565  
566  
567  
568  
569

## References

1. Fu, Q. *et al.* Contribution of stratospheric cooling to satellite-inferred tropospheric temperature trends. *Nature* **429**, doi:10.1038/nature02524 (2004).
2. Cowtan, K. & Way, R. G. Coverage bias in the HadCRUT4 temperature series and its impact on recent temperature trends. *Q. J. R. Meteorol. Soc.* doi: 10.1002/qj.2297 (2014).
3. Forster, P. M. & Shine, K. P. Stratospheric water vapour changes as a possible contributor to observed stratospheric cooling. *Geophys. Res. Lett.* **26**, 3309–3312 (1999).
4. Manabe, S. & Strickler, R. F. Thermal equilibrium of the atmosphere with a convective adjustment. *J. Atmos. Sci.* **21**, 361–385 (1964).
5. Forster, P. M. & Shine, K. P. Assessing the climate impact of trends in stratospheric water vapor. *Geophys. Res. Lett.* **29**, 1086, doi:10.1029/2001GL013909 (2002).
6. Maycock A. C. *et al.* The circulation response to idealized changes in stratospheric water vapor. *J. Clim.*, doi:10.1175/JCLI-D-12-00155.1 (2012).
7. Riese, M. *et al.* Impact of uncertainties in atmospheric mixing on simulated UTLS composition and related radiative effects. *J. Geophys. Res.* **117**, D16305, doi: 10.1029/2012JD017751 (2012).
8. Oltmans, S. J. *et al.* The increase in stratospheric water vapor from balloonborne, frostpoint hygrometer measurements at Washington, D.C., and Boulder, Colorado. *Geophys. Res. Lett.* **27**, doi:10.1029/2000GL012133 (2000).
9. Scherer, M. *et al.* Trends and variability of midlatitude stratospheric water vapour deduced from the re-evaluated Boulder balloon series and HALOE. *Atmos. Chem. Phys.* **8**, 1391–1402, doi:10.5194/acp-8-1391-2008 (2008).
10. Hurst, D. *et al.* Stratospheric water vapor trends over Boulder, Colorado: Analysis of the 30 year Boulder record. *J. Geophys. Res.* **116**, D02306, doi:10.1029/2010JD015065 (2011).
11. Rohs, S. *et al.* Long-term changes of methane and hydrogen in the stratosphere in the period 1978–2003 and their impact on the abundance of stratospheric water vapor. *J. Geophys. Res.* **111**, D14315, doi:10.1029/2005JD006877 (2006).
12. Gettelman, A. *et al.* Multimodel assessment of the upper troposphere and lower stratosphere: Tropics and global trends. *J. Geophys. Res.* **115**, D00M08, doi:10.1029/2009JD013638 (2010).
13. Seidel, D. J. *et al.* Climatological characteristics of the tropical tropopause as revealed by radiosondes. *J. Geophys. Res.* **106**, 7857–7878, doi:10.1029/2000JD900837 (2001).
14. Wang, J. S., Seidel, D. J. & Free, M. How well do we know recent climate trends at the tropical tropopause? *J. Geophys. Res.* **117**, D09118, doi:10.1029/2012JD017444 (2012).

- 570 15. Randel, W.J. et al. Interannual changes of stratospheric water vapor and  
571 correlations with tropical tropopause temperatures. *J. Atmos. Sci.* **61**,  
572 2133-2148, doi:10.1175/1520-0469(2004)061<2133:ICOSWV>2.0.CO;2  
573 (2004).
- 574 16. Fueglistaler, S. et al. The relation between atmospheric humidity and  
575 temperature trends for stratospheric water. *J. Geophys. Res.* **118**, 1052-  
576 1074, doi:10.1002/jgrd.50157 (2013).
- 577 17. Randel, W. J. & Jensen, E. J. Physical processes in the tropical tropopause  
578 layer and their roles in a changing climate. *Nature Geoscience* **6**, 169-176,  
579 doi:10.1038/ngeo1733 (2013).
- 580 18. Hartmann, D.L. et al. Observations: Atmosphere and Surface. In: Climate  
581 Change 2013: The Physical Science Basis. Contribution of Working Group I  
582 to the Fifth Assessment Report of the Intergovernmental Panel on Climate  
583 Change [Stocker, T.F., D. Qin, G.-K. Plattner, M. Tignor, S.K. Allen, J.  
584 Boschung, A. Nauels, Y. Xia, V. Bex and P.M. Midgley (eds.)]. Cambridge  
585 University Press, Cambridge, United Kingdom and New York, NY, USA  
586 (2013).
- 587 19. Fueglistaler, S. & Haynes, P. H. Control of interannual and longer-term  
588 variability of stratospheric water vapor. *J. Geophys. Res.* **110**, D24108,  
589 doi:10.1029/2005JD006019 (2005).
- 590 20. Fujiwara, M. et al. Seasonal to decadal variations of water vapor in the  
591 tropical lower stratosphere observed with balloon-borne cryogenic frost  
592 point hygrometers. *J. Geophys. Res.* **115**, D18304,  
593 doi:10.1029/2010JD014179 (2010).
- 594 21. Dee, D. P. et al. The ERA-Interim reanalysis: configuration and  
595 performance of the data assimilation system. *Q. J. R. Meteorol. Soc.*  
596 **137**, 553-597, doi: 10.1002/qj.828 (2011).
- 597 22. Voemel, H., David, D. E. & Smith, K. Accuracy of tropospheric and  
598 stratospheric water vapor measurements by the cryogenic frost point  
599 hygrometer: Instrumental details and observations. *J. Geophys. Res.* **112**,  
600 D08305, doi:10.1029/2006JD007224 (2007).
- 601 23. Hegglin, M. I. et al. SPARC Data Initiative: Comparisons of water vapour  
602 climatologies from international satellite limb sounders. *J. Geophys. Res.*  
603 **118**, 11824-11846, doi:10.1029/2013JD019614 (2013).
- 604 24. Simmons, A. J. et al. Estimating low-frequency variability and trends in  
605 atmospheric temperature using ERA-Interim. *Q.J.R. Meteorol. Soc.* **140**,  
606 329-353. doi: 10.1002/qj.2317 (2014).
- 607 25. Thomason, L. W. et. al. A revised water vapor product for the Stratospheric  
608 Aerosol and Gas Experiment (SAGE) II version 6.2 data set, *J. Geophys.*  
609 *Res.* **109**, D06312, doi:10.1029/2003JD004465 (2004).
- 610 26. Fueglistaler, S., Stepwise changes in stratospheric water vapor? *J. Geophys.*  
611 *Res.* **117**, D13302, doi:1029/2012JD017582 (2012).
- 612 27. Rosenlof, K. H. & Reid, G. C. Trends in the temperature and water vapor  
613 content of the tropical lower stratosphere: Sea surface connection. *J.*  
614 *Geophys. Res.* **113**, D06107, doi:10.1029/2007JD009109 (2008).

- 615 28. Randel, W. J. Variability and trends in stratospheric temperature and  
616 water vapor. *The Stratosphere: Dynamics, Transport and Chemistry*, S.  
617 Polvani, and Waugh, Eds., American Geophysical Union, 123-135 (2010).
- 618 29. Kelly, K. K. et al. Dehydration in the lower Antarctic stratosphere during  
619 late winter and early spring, 1987. *J. Geophys. Res.* **94**, 317–11,357 (1989).
- 620 30. Solomon, S. et al. Contributions of stratospheric water vapor changes to  
621 decadal variation in the rate of global warming. *Science* **327**, 1219–1222,  
622 doi:10.1226/science.1182488 (2010).
- 623 31. Jones, A. et al. Evolution of stratospheric ozone and water vapour time  
624 series studied with satellite measurements. *Atmos. Chem. Phys.* **9**, 6055-  
625 6075, doi:10.5194/acp-9-6055-2009, 2009 (2012).
- 626 32. Garfinkel, C. I., D. W. Waugh, L. D. Oman, L. Wang, & M. M. Hurwitz.  
627 Temperature trends in the tropical upper troposphere and lower  
628 stratosphere: Connections with sea surface temperatures and implications  
629 for water vapor and ozone. *J. Geophys. Res.* **118**, 9658–9672,  
630 doi:10.1002/jgrd.50772 (2013).
- 631 33. Le Texier, H., Solomon, S., & Garcia, R. R. The role of molecular hydrogen  
632 and methane oxidation in the water vapor budget of the stratosphere. *Q. J.*  
633 *R. Meteorol. Soc.* **114**, 281-295 (1988).
- 634 34. Dessler, A.E. et al. An examination of the total hydrogen budget of the  
635 lower stratosphere. *Geophys. Res. Lett.* **21**, 2563-2566 (1994).
- 636 35. Ray, E. A. et al. Evidence for changes in stratospheric transport and mixing  
637 over the past three decades based on multiple data sets and tropical leaky  
638 pipe analysis. *J. Geophys. Res.* **115**, D21304, doi:10.1029/2010JD014206  
639 (2010).
- 640 36. Engel, A. et al. Age of stratospheric air unchanged within uncertainties  
641 over the past 30 years. *Nat. Geosci.* **2**, 28–31, doi:10.1038/Ngeo388  
642 (2009).
- 643 37. Bönisch, H., Engel, A., Birner, T., Hoor, P., Tarasick, D. W., & Ray, E. A. On  
644 the structural changes in the Brewer-Dobson circulation after 2000.  
645 *Atmos. Chem. Phys.* **11**, 3937-3948, doi:10.5194/acp-11-3937-2011  
646 (2011).
- 647 38. Butchart, N. et al. Chemistry–climate model simulations of twenty-first  
648 century stratospheric climate and circulation changes. *J. Climate* **23**, 5349–  
649 5374, doi:10.1175/2010JCLI3404.1 (2010).
- 650 39. McLandress, C. & Shepherd, T. G. Simulated anthropogenic changes in the  
651 Brewer-Dobson circulation, including its extension to high latitudes. *J.*  
652 *Clim.* **22**, 1516–1540 (2009).
- 653 40. Scinocca, J. F. et al. Technical Note: The CCCma third generation AGCM and  
654 its extension into the middle atmosphere. *Atmos. Chem. Phys.* **8**, 7055-  
655 7074, doi:10.5194/acp-8-7055-2008 (2008).
- 656 41. Jensen, E. J. et al. Ice nucleation and dehydration in the Tropical  
657 Tropopause Layer. *P. Natl. Acad. Sci.* **110**, 2041–2046,  
658 doi:10.1073/pnas.1217104110 (2013).

659 42. Hegglin, M. I. et al. Multimodel assessment of the upper troposphere and  
660 lower stratosphere: Extratropics. *J. Geophys. Res.* **115**, D00M09,  
661 doi:10.1029/2010JD013884 (2010).  
662 43. Toohey, M. et al. Characterizing sampling biases in the trace gas  
663 climatologies of the SPARC Data Initiative. *J. Geophys. Res.* **118**,  
664 doi:10.1002/jgrd.50874 (2013).  
665 44. Damadeo, R. P. et al. SAGE version 7.0 algorithm: application to SAGE II.  
666 *Atmos. Meas. Tech.* **6**, 3539-3561, doi:10.5194/amt-6-3539-2013 (2013).  
667 45. De Mazière, M. et al. Validation of ACE-FTS v2.2 methane profiles from the  
668 upper troposphere to the lower mesosphere. *Atmos. Chem. Phys.* **8**, 2421-  
669 2435, doi:10.5194/acp-8-2421 (2008).  
670 46. Hurst, D.F. et al. Validation of Aura Microwave Limb Sounder stratospheric  
671 water vapor measurements by the NOAA frost point hygrometer. *J.*  
672 *Geophys. Res.* **119**, doi:10.1002/2013JD020757 (2014).  
673 47. Santer, B. D. et al. Statistical significance of trends and trend differences in  
674 layer-average atmospheric temperature time series. *J. Geophys. Res.* **105**,  
675 7337–7356 (2000).  
676  
677  
678  
679  
680  
681  
682  
683  
684  
685  
686  
687